

Efficient and Ambient-Air-Stable Solar Cell with Highly Oriented 2D@3D Perovskites

Tao Ye, Annalisa Bruno, Guifang Han, Teck Ming Koh, Jia Li, Nur Fadilah Jamaludin, Cesare Soci, Subodh G. Mhaisalkar, and Wei Lin Leong*

3D organic–inorganic lead halide perovskites have shown great potential in efficient photovoltaic devices. However, the low stability of the 3D perovskite layer and random arrangement of the perovskite crystals hinder its commercialization road. Herein, a highly oriented 2D@3D ((AVA)₂PbI₄@MAPbI₃) perovskite structure combining the advantages of both 2D and 3D perovskite is fabricated through an in situ route. The highest power conversion efficiency (PCE) of 18.0% is observed from a 2D@3D perovskite solar cell (PSC), and it also shows significantly enhanced device stability under both inert (90% of initial PCE for 32 d) and ambient conditions (72% of initial PCE for 20 d) without encapsulation. The high efficiency of 18.0% and nearly twofold improvement of device stability in ambient compared with pure 3D PSCs confirm that such 2D@3D perovskite structure is an effective strategy for high performance and increasing stability and thus will enable the timely commercialization of PSCs.

1. Introduction

Organic–inorganic lead halide perovskite solar cells (PSCs) have been regarded as one of the most promising photovoltaic technologies due to their unique optical and electrical properties such as high absorption coefficient ($\approx 10^4 \text{ cm}^{-1}$),^[1,2] optical tunability,^[3–5] long-range charge transport,^[6–8] as well as low-cost solution processability.^[6,7,9,10] Organic–inorganic lead halide perovskite can be represented by the general formula, APbX₃ [A = MA(CH₃NH₃, methylammonium), or FA (NH = CHNH₃, formamidinium); X = Cl, Br, and I] and a certified power conversion efficiency (PCE) as high as 22.7% has already been achieved.^[11] The high efficiencies encourage growing research efforts and investment


from both industry and academia to realize their commercialization potential. However, there are issues related to device stability under operating condition which are a major bottleneck for commercialization.^[12]

The structural and electrical properties of perovskite can be tuned by varying the size and proportion of the organic cations. A large or small organic cation can cause the whole lattice to expand or contract, influencing the bandgap.^[13–15] In the case of the popular MAPbI₃, the perovskite material is sensitive to moisture, oxygen, and thermal stress.^[16–18] For instance, it degrades and hydrolyzes in humid environment, resulting in the destruction of the lattice structure. Therefore, newer perovskite compositions which show good stability under ambient air have to be pursued. In this respect, a variety of studies

have focused on the development of 2D layered structure by introducing larger sized hydrophobic organic cations such as phenethylammonium and butylammonium.^[19,20] These 2D phases have shown superior moisture stability over solely 3D MAPbI₃. However, their increased bandgap, unoptimized film morphology, and out-of-plane charge transport arising from insulating organic spacers resulted in relatively low solar cell efficiency (PCE < 13%).^[20–22] More recent efforts combined 3D and 2D halide perovskite structures to take advantage of the good photovoltaic properties of the 3D perovskites and ambient air stability of the 2D perovskite.^[23–26] But it is still a challenge for 2D/3D perovskites to achieve high efficiency comparable to 3D perovskites and good ambient stability at the same time.^[24,27,28]

Dr. T. Ye, Dr. A. Bruno, Dr. G. Han, Dr. T. M. Koh, Dr. J. Li, N. F. Jamaludin, Prof. S. G. Mhaisalkar, Prof. W. L. Leong
Energy Research Institute @ NTU (ERI@N)
Nanyang Technological University
50 Nanyang Drive, X-Frontiers Block, Level 5, Singapore 637553, Singapore
E-mail: wleong@ntu.edu.sg

N. F. Jamaludin
Interdisciplinary Graduate School
Nanyang Technological University
50 Nanyang Avenue, Singapore 639798, Singapore

 The ORCID identification number(s) for the author(s) of this article can be found under <https://doi.org/10.1002/adfm.201801654>.

N. F. Jamaludin, Prof. S. G. Mhaisalkar
School of Materials Science and Engineering
Nanyang Technological University
50 Nanyang Avenue, Singapore 639798, Singapore

Prof. C. Soci
Division of Physics and Applied Physics
School of Physical and Mathematical Sciences
Nanyang Technological University
21 Nanyang Link, Singapore 637371, Singapore

Prof. W. L. Leong
School of Electrical and Electronic Engineering
School of Chemical and Biomedical Engineering
Nanyang Technological University
50 Nanyang Avenue, Singapore 639798, Singapore

DOI: 10.1002/adfm.201801654

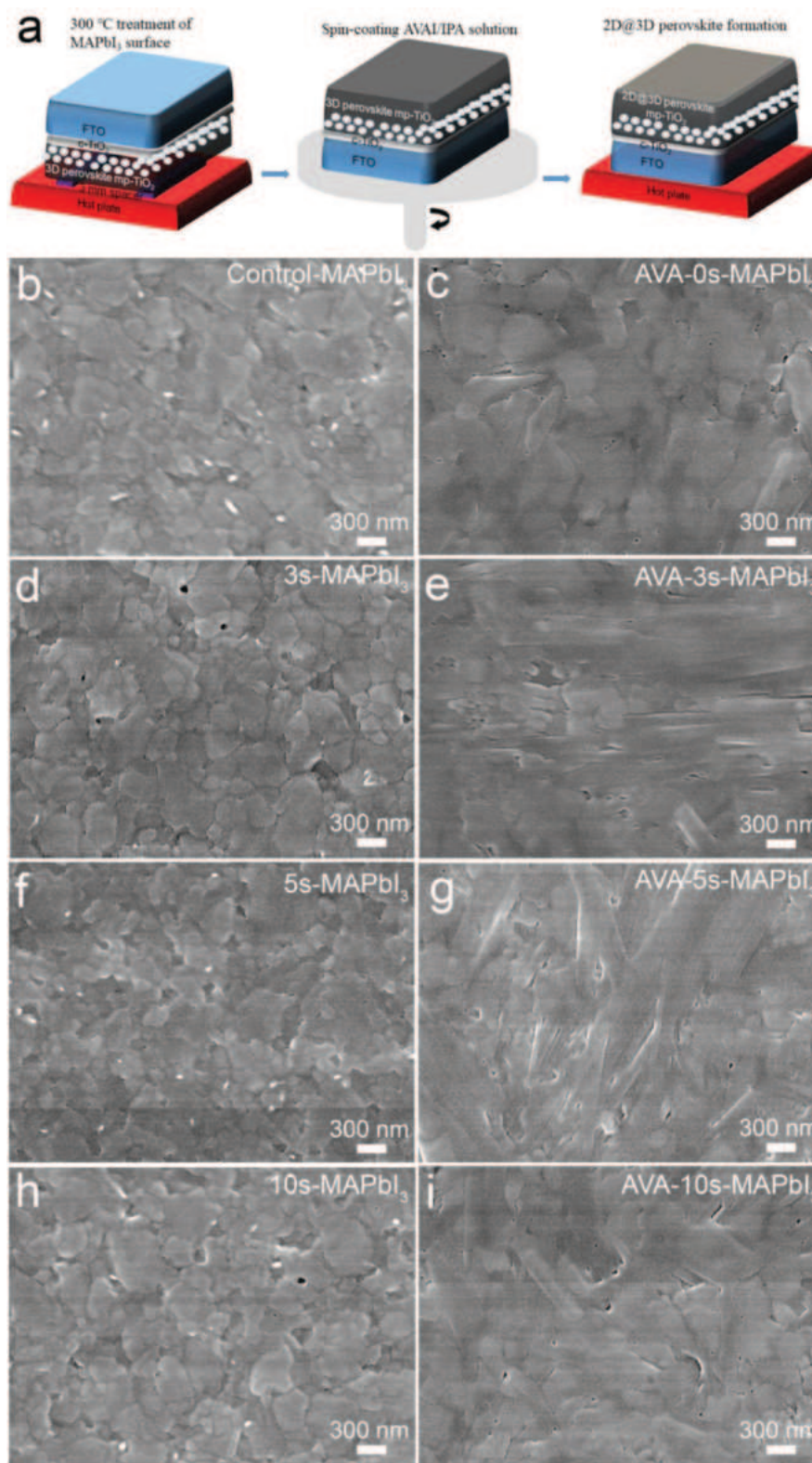


Figure 1. a) The schematic of the 2D@3D perovskites deposition processes. The surface SEM images of b) as-prepared 3D perovskite film (control), c) 2D@3D perovskite film with AVAI directly deposited on the 3D perovskite film (AVA-0s-MAPbI₃), d) 3D perovskite film with 3 s high-temperature (300 °C) treatment, e) 2D@3D perovskite film with AVAI deposited on the (d) perovskite film (AVA-3s-MAPbI₃), f) 3D perovskite film with 5 s high-temperature (300 °C) treatment, g) 2D@3D perovskite film with AVAI deposited on the (f) perovskite film (AVA-5s-MAPbI₃), h) 3D perovskite film with 10 s high-temperature (300 °C) treatment, i) 2D@3D perovskite film with AVAI deposited on the (h) perovskite film (AVA-10s-MAPbI₃).

Herein, we demonstrate that, by utilizing an in situ growth route to fabricate 2D@3D perovskite light absorbers, higher PCE of 18.0% and enhanced device stability (retaining 72% of their initial efficiency after 20 d, \approx 40% relative humidity (RH)) as compared with their 3D counterparts, MAPbI₃ (PCE = 17.3%, retained 40% of their initial efficiency after 20 d) can be achieved. We adopted a modified flash-annealing method on the 3D perovskite surface to release the organic halide CH₃NH₃I, leaving the inorganic Pb–I framework at the surface. We next incorporated 5-aminovaleric acid iodide, (HOOC(CH₂)₄NH₃I, AVAI), by casting the additive solution on top of the annealed films, which resulted in the formation of 2D perovskite structure. This 2D@3D perovskite fabrication approach provides a simple and universal solution for efficient and ambient-air-stable perovskite film and device fabrication. Our work illustrates that engineering the interfaces between 2D and 3D perovskite phases is crucial to simultaneously achieve high performing and stable PSCs.

2. Results and Discussion

The 3D MAPbI₃ light absorber layers with highly oriented crystal structure along (110) direction were fabricated with a new dimethyl sulfoxide (DMSO)-enriched recipe.^[24] The main effect of DMSO is its strong coordination with Pb element to form an adduct intermediate phase of MA₂Pb₃I₈(DMSO)₂ which will slow down the crystallization of perovskite and form larger perovskite crystals. As shown in **Figure 1b**, the DMSO-enriched recipe does produce dense and uniform perovskite films. To form the 2D@3D perovskite light absorbers, the 3D perovskite films were first annealed at high temperature (300 °C) for a short time (3, 5, or 10 s), then spun-cast by AVAI/isopropanol (IPA) solution (details can be in the Experimental Section). It is important to note that this high-temperature flash annealing is done with the MAPbI₃ films in close contact with the hotplate (i.e., the MAPbI₃/mp-TiO₂/TiO₂/FTO sample was briefly placed \approx 3 mm above the hotplate). The surfaces of 3D perovskites have been shown to be defective and several amine functional molecules were reported to passivate the surface defects of the perovskite films.^[25,29] Towards that end, we employed a high temperature flash-annealing process, where the surface MAI can be removed from the Pb–I framework which subsequently interacts with the AVAI molecules to yield a better interface between the 3D and 2D phases. The deposition of the AVAI solution results in the formation of 2D perovskite, possibly into a (AVA)₂PbI₄ structure^[12] at the surface, forming the 2D@3D perovskites. The amine and carboxyl functional groups of AVAI can interact with the 3D perovskite through hydrogen-to-halogen bonding, allowing better 2D/3D interfaces and hence lower recombination at the 2D/3D interface. The 2D@3D perovskite fabrication process is illustrated in **Figure 1a**. **Figure 1b,d,f,h** shows the surface morphologies of the 3D perovskite for different durations of the high-temperature treatment (300 °C for 3, 5, or 10 s). Similar crystal features are observed, indicating the surface morphologies of the 3D perovskite are unaffected by the high-temperature flash-annealing treatment. This is reasonable since the annealing time is very short (3–10 s) and the thermal conductivity of the

3D MAPbI₃ layer is very low, according to recent reports.^[30–32] The AVAI solutions are then spun-cast on top of these flash-annealed 3D perovskite films. Herein after, we denote the 2D@3D films flashed-annealed for various times with AVAI as: AVA-0s-MAPbI₃, AVA-3s-MAPbI₃, AVA-5s-MAPbI₃, and AVA-10s-MAPbI₃. The surface features after deposition of the AVAI are shown in **Figure 1c,e,g,i**, where more compact and smooth perovskite surfaces are observed. Furthermore, the X-ray diffraction (XRD) results show that the surface MAI has been partially removed during the high-temperature flash-annealing process due to the more pronounced 12.7° PbI₂ peak for 10 s thermal treatment (**Figure S1**, Supporting Information). There is no clear evidence of the PbI₂ peak for shorter annealing time of 3–5 s. We postulate the reason is that only a small amount of MAI may be removed from the defect sites (grain boundaries) during the high-temperature flash-annealing treatment and our device results showed that this small amount of MAI removal is crucial for the subsequently deposited AVAI to react with the residual PbI₂ and form more stable 2D perovskites at these sites.

Optical properties of the pure and 2D@3D perovskite layers were investigated and the results are shown in **Figure 2**. **Figure 2a** shows the UV–vis absorption of the pure 3D and 2D@3D perovskites. After AVAI deposition the band edges of the absorption spectra are almost invariant at \approx 788 nm (the corresponding Tauc plots are also presented in **Figure S2** in the Supporting Information). A remarkable 2D feature at \approx 424 nm is also clearly visible, in agreement with previously reported results.^[12] The 2D@3D perovskite films fabricated under the different high-temperature flash-annealing conditions also affect the light absorption properties. When AVAI is directly deposited on top of the 3D MAPbI₃ layer (without the flash-annealing treatment), the absorption of the sample decreases rapidly in the 447–800 nm range. In contrast, the absorption of the 2D@3D perovskite samples slowly increased with increasing annealing time. The strongest optical absorption was obtained from the AVA-5s-MAPbI₃ sample, most likely due to the better formation of the 2D@3D perovskite structure. **Figure 2b** shows the steady-state photoluminescence (PL) spectra of 3D perovskite and AVA-5s-MAPbI₃ 2D@3D perovskites (excitation at 405 nm). The PL yield of the 2D@3D perovskite is much higher than the control sample, which indicates reduced non-radiative recombination processes. This correlates well with our postulation that the amine and carboxyl functional groups of AVAI can interact well with the 3D perovskites, allowing better 2D/3D interfaces and eliminate the trap states at the 3D perovskite surface. To further confirm the presence of 2D phase in the top surface of 3D perovskites, PL signals from both bottom and top of the substrates for AVA-5s-MAPbI₃ 2D@3D perovskite layer were measured and compared (**Figure 2c**). When the sample was excited by 405 nm light from the top, a weak PL emission of around 456 nm was obtained, similar to previous reports.^[12] No obvious PL emission at 450–470 nm was obtained when similar measurements with bottom excitation are done using the same excitation wavelength. This suggests the 2D perovskite phase is mostly retained at the top layer of the sample. Time-resolved PL (TRPL) dynamics of the 765 nm peak for the pure 3D perovskite as well as the AVA-5s-MAPbI₃ 2D@3D perovskite were also examined (**Figure 2d**).

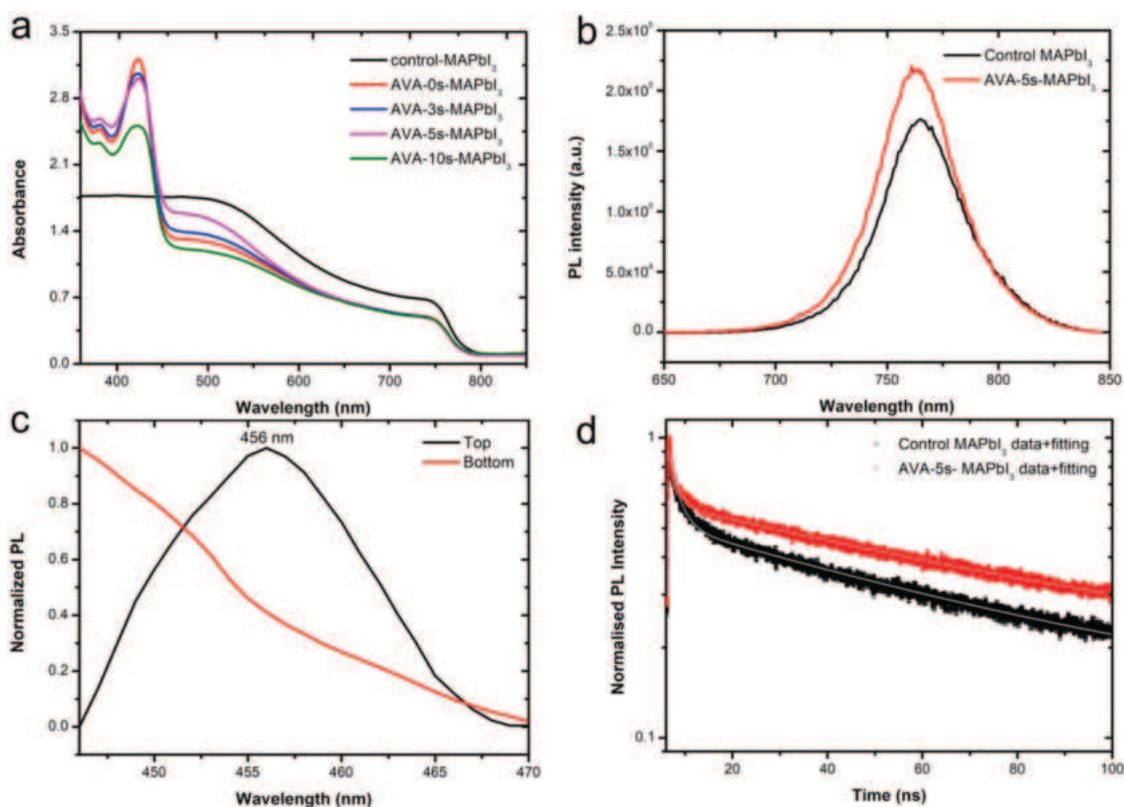


Figure 2. Optical characterization results of the perovskite samples. a) UV-vis optical absorption spectra of the control 3D perovskite films and 2D@3D perovskite films with different flash-annealing duration (AVA-0s-MAPbI₃, AVA-3s-MAPbI₃, AVA-5s-MAPbI₃, and AVA-10s-MAPbI₃). b) PL spectra, excitation at 405 nm, of the control 3D perovskite and 2D@3D perovskite (AVA-5s-MAPbI₃). c) Normalized PL spectra, excitation at 405 nm, of the AVA-5s-MAPbI₃ perovskite from the top perovskite layer and from the bottom substrate side. d) PL dynamics of the bulk perovskite (with fitting) of the pure 3D and 2D@3D (AVA-5s-MAPbI₃) perovskite samples, exciting at 405 nm.

When excited at 405 nm, the fluorescence lifetime of the pure mixed 2D@3D system is long lived, with an average lifetime of 52.5 ns. The PL lifetime is significantly shorter (39.7 ns) in the 3D perovskite, as summarized in Table S1 in the Supporting Information. This observation correlates well with the steady-state PL, which implies that the formation of the 2D phase heals the surface defects of the 3D phase, therefore reducing nonradiative recombination.^[29,33–36]

PSCs based on these 2D@3D perovskites were fabricated—the detailed processes of the solar device fabrication can be found in Figure S3 in the Supporting information and in the Experimental Section. Figure 3a,c shows the cross-sectional scanning electron microscope (SEM) images of the pure 3D and AVA-5s-MAPbI₃ 2D@3D PSC devices. While the perovskite layers in the two devices show similar film thickness, no clear interface (gap) was observed in the 2D@3D perovskite layer. A comparison of XRD measurements of the pure 3D and 2D@3D perovskites with different high-temperature flash-annealing treatments can be seen in Figure 3b,d. For the pure 3D perovskites, a strong (110) peak ($\approx 14.1^\circ$) is seen in the XRD patterns (Figure 3b), while other MAPbI₃ characteristic peaks are not present. This implies the synthesized perovskite crystals are highly oriented and that the crystal structure of the MAPbI₃ films does not change substantially upon high-temperature flash annealing. We note that this is the first observation

of highly oriented perovskite crystals using the modified DMSO recipe and corresponding XRD patterns in 3D perovskites. The addition of DMSO has thus proven to be an effective method in slowing down the crystal growth and led to highly oriented perovskites.^[24,37] Recent results^[9,24,38] have also suggested that high-efficiency PSC requires such highly oriented perovskite crystals to take advantage of their enhanced charge carrier injection/transport properties and reduced surface area of the grain boundaries. After AVAI deposition, the presence of an additional (001) peak ($\approx 4.8^\circ$) which is characteristic of the 2D perovskite-(AVA)₂PbI₄ can be seen in Figure 3d (the XRD spectra of the 2D perovskite-(AVA)₂PbI₄ are also measured, as shown in Figure S4 in the Supporting Information).^[12,39] We note that other characteristic diffraction peaks for (AVA)₂PbI₄ are not observed in the 2D@3D films, possibly due to the 2D perovskite layers being too thin to be detected in our regular XRD measurements.

The current density–voltage (*J*–*V*) characterizations measured under simulated AM 1.5 radiation of our best cells with different perovskite light absorbers are shown in Figure 4a. The detailed *J*–*V* parameters of the devices can also be found in Table 1. A high PCE of 17.3% can be achieved for the 3D MAPbI₃, while the efficiency reduces to 14.4% for direct deposition of the AVAI (without flash-annealing treatment, AVA-0s-MAPbI₃). As the high-temperature flash-annealing

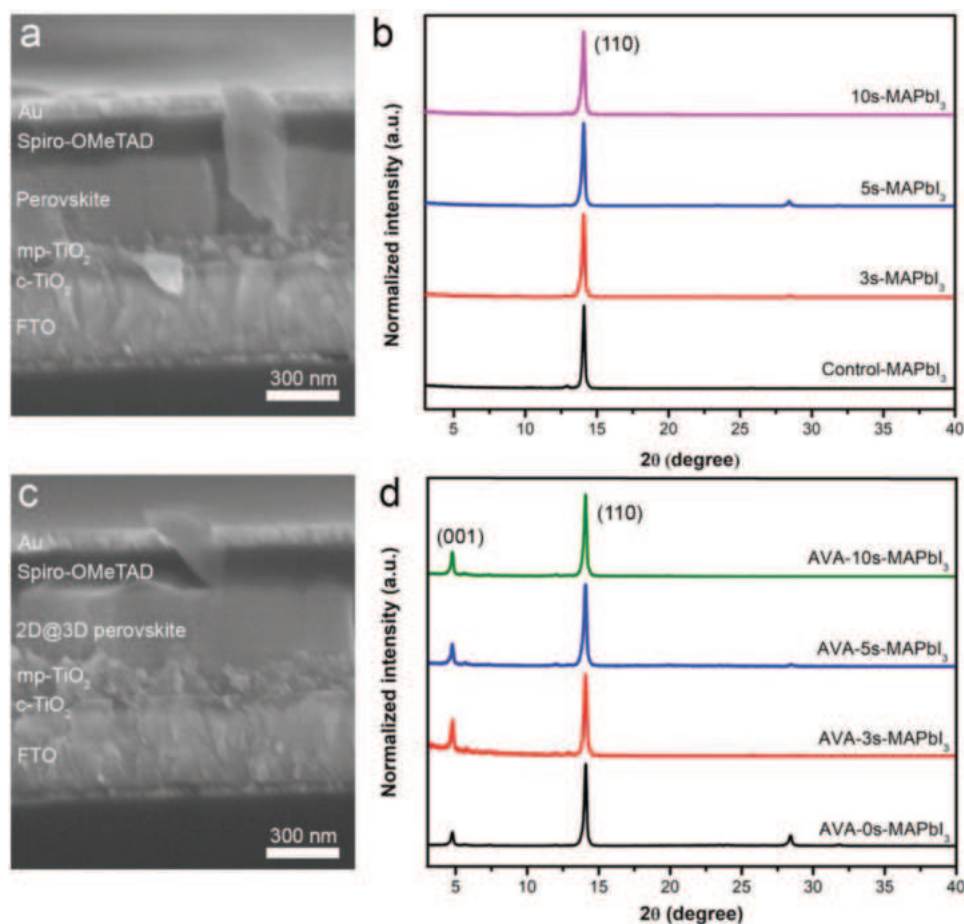


Figure 3. a) Cross-section SEM image of the control 3D perovskite device. b) XRD patterns of different 3D perovskite samples annealed at 300 °C for various duration time (without AVAI deposition). c) Cross-section SEM image of the AVA-5s-MAPbI₃ 2D@3D perovskite device. d) XRD results of 2D@3D perovskite samples with different flash-annealing conditions and AVAI deposition. (a,c) clearly show the formation of highly oriented (perpendicular to the TiO₂ substrates) 3D perovskite crystals. c-TiO₂: compact TiO₂ layer; mp-TiO₂: mesoporous TiO₂ layer; FTO: fluorine doped tin oxide substrate; spiro-OMeTAD: 2,2',7,7'-tetrakis(*N,N*-di-*p*-methoxyphenylamine)-9,9'-spirobifluorene.

time increased from 3 to 5 s, the PCE improved to 16.8% and 18.0%, respectively. Specifically, the AVA-5s-MAPbI₃ 2D@3D perovskite device, which has the highest PCE of 18.0% and also correlates well with the observed higher PL yield, has high short-circuit current density (J_{sc}) of 22.3 mA cm⁻², open-circuit voltage (V_{oc}) of 1.06 V, and fill factor (FF) of 0.76. The results also indicated that the thickness of the 2D layer was low to an extent that allowed efficient charge transport from the 3D perovskite to the hole transporting layer, leading to the relatively high photovoltaic parameters. The forward scan and dark J - V curves of the AVA-5s-MAPbI₃ 2D@3D perovskite device can be found in Figure S5 in the Supporting Information. When the high-temperature annealing time increases to 10 s, the PCE decreases rapidly to just 14.5%, most likely due to increased MAI removal and excessive residual PbI₂ on the perovskite surface after flash annealing, which increases crystal disorder after AVAI deposition. The AVAI (2D perovskite) stacking and perovskite crystal disorder at the perovskite/spiro-OMeTAD interface may affect the charge carrier injection/transport within the system, lowering device performance. We also compared the device performance of the pure 3D perovskite that undergo

the best flash-annealing treatment of 5 s, but without the AVAI deposition. The device efficiency is found to be lower than AVA-5s-MAPbI₃ 2D@3D PSCs (Figure S6, Supporting Information), mainly due to the differences in J_{sc} . Devices prepared via direct deposition of the AVAI (without flash-annealing treatment, AVA-0s-MAPbI₃) also showed poorer performance. Thus, both the flash-annealing treatment and subsequent deposition of AVAI on top of 3D MAPbI₃ (AVA-5s-MAPbI₃) are crucial for achieving high-efficiency mixed 2D@3D perovskites. Corresponding to the J_{sc} trends, the internal photon-to-electron conversion efficiency (IPCE) spectra showed an increase over the entire wavelength range for the best 2D@3D device (AVA-5s-MAPbI₃), with broad photoresponse from 400 to 750 nm (Figure 4b). Figure 4c presents the PCE distribution of the five different groups of devices, where the PCE variation among these groups follows a similar trend as the performance change of our best cells.

Finally, the stability of perovskite films and solar devices were investigated. We first looked at the thermal stability of the control and 2D@3D perovskite films by deliberately subjecting the perovskite samples (FTO/c-TiO₂/mp-TiO₂/perovskite) to 100 °C

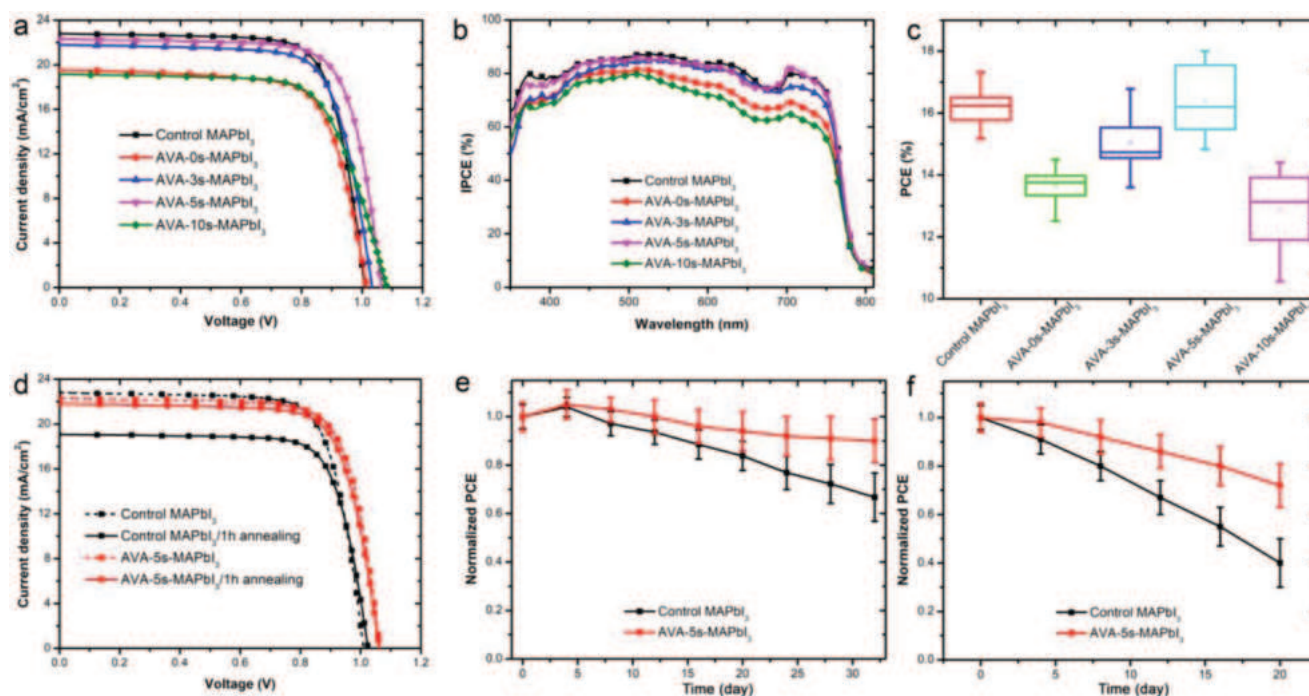


Figure 4. a) J - V results of the champion cells with different perovskite light absorbers under simulated AM 1.5 radiation and the b) corresponding IPCE spectra of the champion cells. c) PCE of the devices extracted from J - V measurements for the different groups of PSCs with and without AVAI deposition, 20 devices have been fabricated for each group. d) Thermal stability study. Comparison of J - V results of the control 3D perovskite fabricated with and without subjecting to thermal stress (perovskite film annealed at 100 °C for 1 h before making full devices). Similar comparison of J - V results is done for the champion 2D@3D perovskite (AVA-5s-MAPbI₃) which showed higher thermal stability. Stability measurements of the control and AVA-5s-MAPbI₃ PSCs at e) argon atmosphere and f) ambient ($\approx 40\%$ RH) and room temperature of 25 °C.

for 1 h, followed by completing the fabrication of the PSCs by deposition of spiro-OMeTAD and the Au electrode. The AVA-5s-MAPbI₃ 2D@3D perovskite device retains comparable efficiency ($\approx 17.4\%$), but the pure 3D perovskite device yields only 14.9% efficiency (the J - V curves are shown in Figure 4d and the detailed photovoltaic parameters can be seen in Table S2, Supporting Information). The surface SEM images of the two perovskite films in Figure S7 in the Supporting Information show that pinholes emerged in the pure 3D perovskite film after annealing the films at 100 °C for 1 h, while the AVA-5s-MAPbI₃ perovskite film remains unaffected. This provides strong evidence of the enhanced thermal stability in the hybrid 2D@3D perovskites. Next, the moisture stability of the two perovskite films was measured by placing the samples on top of a beaker of hot water, to simulate a relative humidity of $\approx 93\%$. Optical images show that the moisture stability of the AVA-5s-MAPbI₃ 2D@3D perovskite film is higher than that of the control

sample, where the 3D perovskite starts to turn yellow after 2 s of exposure to moisture whereas the 2D@3D perovskite film still remains black (Figure S8, Supporting Information).

The device stability of the 3D perovskite and AVA-5s-MAPbI₃ 2D@3D perovskite were also studied for comparison (Figure 4e,f). We find that when the devices are stored in an argon-filled glovebox for 32 d, the AVA-5s-MAPbI₃ 2D@3D perovskite device retains 90% of its initial PCE, but the PCE of the 3D MAPbI₃ device drops to 67% of its initial value. In addition, the PCE of the 3D MAPbI₃ device decreases much faster to 40% of its initial PCE under $\approx 40\%$ RH after 20 d, while under the same ambient condition, the 2D@3D device (AVA-5s-MAPbI₃) holds 72% of the initial PCE. This 2D@3D perovskite synthesis method can thus be utilized to improve the thermal, moisture, and oxygen stabilities of both the perovskite films and devices.

Table 1. Comparison of device performance parameters for control and 2D@3D perovskite-based champion PSCs.

	V_{oc} [V]	J_{sc} [mA cm ⁻²]	FF	PCE [%]
Control MAPbI ₃	1.01	22.8	0.75	17.3
AVA-0s-MAPbI ₃	1.02	19.54	0.74	14.4
AVA-3s-MAPbI ₃	1.04	21.8	0.74	16.8
AVA-5s-MAPbI ₃	1.06	22.3	0.76	18.0
AVA-10s-MAPbI ₃	1.08	19.2	0.70	14.5

3. Conclusion

In conclusion, we demonstrated an in situ method to fabricate the 2D@3D perovskite light absorber. Using a new DMSO-enriched recipe, MAPbI₃ film with highly oriented perovskite crystals was obtained. The unique 2D@3D perovskite obtained by treating the 3D perovskite films with rapid thermal annealing and subsequently coating them with AVAI combines the advantages of both 2D perovskites (e.g., enhanced thermal, moisture, and oxygen stability) and 3D perovskites (e.g., high

optical absorption, long-range charge transport, and efficient charge collection). The 2D perovskite also performs the role of passivating the surface defects of the 3D perovskite and therefore reducing nonradiative recombination. The highest PCE of 18.0% has been attained with an AVA-5s-MAPbI₃ 2D@3D perovskite device with improved stability in both inert (90% of initial PCE for 32 d) and ambient conditions (72% of initial PCE for 20 d). This novel 2D@3D perovskite fabrication method is extremely promising for the realization of highly efficient and ambient-air-stable PSCs suitable for large-scale production and deployment in the field.

4. Experimental Section

Materials: Unless specified otherwise, all chemicals were purchased from Sigma-Aldrich. Mesoporous TiO₂ paste, MAI, and AVAI were purchased from Dyesol. PbI₂ was purchased from TCI.

Device Fabrication: FTO glass substrate (<15 Ω square⁻¹, NSG) was cleaned with detergent, DI water, ethanol (Sigma-Aldrich), IPA (Sigma-Aldrich) and treated with UV ozone treatment at 100 °C for 10 min. An \approx 50 nm TiO₂ layer was deposited on top of the FTO by spin-coating TiO₂ precursor solution at 5000 rpm for 30 s. Then, it was heated at 450 °C for 30 min in air. To prepare the TiO₂ precursor solution, titanium isopropoxide (1 mL, Sigma-Aldrich) and 12 M HCl solution (10 μ L, Sigma-Aldrich) were diluted in ethanol (10 mL). Then an \approx 150 nm mesoporous TiO₂ layer was deposited by spin coating a 30 nm TiO₂ nanoparticle paste (Dyesol) in ethanol (1:6 in weight ratio) at a speed of 5500 rpm for 30 s. The substrate was then annealed at 500 °C for 20 min. The TiO₂ layers were treated with a diluted TiCl₄ aqueous (50×10^{-3} M in DI water, Wako Pure Chemical Industries) solution. Next, perovskite film was deposited on the substrate by two-step spin-coating process using warm (50–60 °C) precursor solution in an argon-filled glovebox. First, 1000 rpm for 10 s; second, 4000 rpm for 40 s, then chlorobenzene (110 μ L, Sigma-Aldrich) was dropped in 23–26 s during the second spin-coating process. The substrate was then heated at 100 °C for 15 min. The precursor solution was prepared by dissolving MAI (0.214 g) and PbI₂ (0.622 g) in anhydrous *N,N*-dimethylformamide (0.2 mL, Sigma-Aldrich) and anhydrous dimethylsulfoxide (0.8 mL, Sigma-Aldrich). To form the 2D@3D perovskite layer, the prepared MAPbI₃ surface was treated with short time (0, 3, 5, and 10 s) under high temperature (300 °C) and then AVAI/IPA (3 mg mL⁻¹) solution has been spin coated on top of the perovskite film at 3000 rpm for 30 s. The substrate was then heated at 100 °C for 4 min. Spiro-OMeTAD (Sigma-Aldrich) was further deposited by spin coating at 3000 rpm for 30 s. The spiro-OMeTAD solution was prepared by dissolving 74 mg spiro-OMeTAD, 28.5 μ L 4-*tert*-butylpyridine (Sigma-Aldrich), 17.5 μ L of a stock solution of 520 mg mL⁻¹ lithium bis (trifluoromethylsulfonyl) imide (Sigma-Aldrich) in acetonitrile (Sigma-Aldrich), and 29 μ L of a stock solution of 200 mg mL⁻¹ tris(2-(1H-pyrazol-1-yl)-4-*tert*-butylpyridine)-cobalt(III) tris(bis(trifluoromethylsulfonyl) imide) (Sigma-Aldrich) in acetonitrile in 1 mL anhydrous chlorobenzene. Finally, 80 nm of gold was deposited as an electrode by thermal evaporation.

Characterization: XRD experiments were conducted by a Bruker AXS (D8 ADVANCE) X-ray diffractometer with Cu K radiation ($\lambda = 1.54$ Å) and the perovskite samples for XRD study were prepared following exactly the same procedures as for the device fabrication. For the pure 2D perovskites for XRD measurements, the precursor solution was prepared by dissolving AVAI (0.098 g) and PbI₂ (0.092 g) in anhydrous *N,N*-dimethylformamide (0.05 mL) and anhydrous dimethylsulfoxide (0.15 mL). *J*-*V* characteristics were measured by using a solar simulator (SAN-EI Electric XEC-301S) and a Keithley 2612A digital source meter under standard simulated AM 1.5 illumination, and the light intensity was calibrated by using a standard reference silicon cell (Newport). The solar cells were masked with metal apertures to define the active areas which were typically 0.09 cm². IPCE was recorded by using a PVE300

(Bentham), with a dual xenon/quartz halogen light source, measured in DC mode without additional light bias. The light intensity was calibrated using a silicon calibrated detector (Newport). The surface and cross-section morphologies of the samples were investigated by a SEM (JEOL JSM-7001F) at 10 kV. UV–vis optical absorption spectra of the perovskite samples were acquired with a UV-3600 (Shimadzu) spectrophotometer. PL spectra were recorded by using FluoroMax-4 (HORIBA industry) and the emission for the number of the absorbed photons at the excitation wavelength has been corrected. The perovskite samples for PL measurements were deposited on the clean glass substrates with the same method of solar cell fabrication. TRPL was measured in a micro-PL setup, employing a Nikon microscope, and using a Picoquant PicoHarp 300 time-correlated single photon counting (TCSPC) system. The samples were excited using a ps-pulsed laser diode emitting at 405 nm with 40 MHz repetition rate (Picoquant P-C-405B, < 1 μ J cm⁻²) through a 20 \times magnification lens and NA = 0.3. The output signal is then fiber coupled to Acton SP-2300i monochromator (300 mm focal length) for spectral selection of the emission light. Another optical fiber connected to the output of the monochromator is used to couple spectral separated output light to an avalanche diode that is synchronized with the excitation laser via the TCSPC electronic. Overall, the full width at half maximum of the system instrument respond function is around 50 ps.

Supporting Information

Supporting Information is available from the Wiley Online Library or from the author.

Acknowledgements

W.L.L. would like to acknowledge funding support from her NTU start-up grant (M4081866) and the Ministry of Education (MOE) under AcRF Tier 1 grant (RG 165/16). S.G.M. acknowledges funding from MOE Tier 2 grant (MOE2016-T2-2-012). Research was partly supported by the Singapore National Research Foundation (CRP Award No. NRF-CRP14-2014-03).

Conflict of Interest

The authors declare no conflict of interest.

Keywords

interfaces, organic lead halide perovskite, oriented perovskite, solar cells

Received: March 5, 2018

Revised: April 18, 2018

Published online:

- [1] A. Kojima, K. Teshima, Y. Shirai, T. Miyasaka, *J. Am. Chem. Soc.* **2009**, *131*, 6050.
- [2] J. H. Im, C. R. Lee, J. W. Lee, S. W. Park, N. G. Park, *Nanoscale* **2011**, *3*, 4088.
- [3] J. H. Noh, S. H. Im, J. H. Heo, T. N. Mandal, S. I. Seok, *Nano Lett.* **2013**, *13*, 1764.
- [4] M. M. Lee, J. Teuscher, T. Miyasaka, T. N. Murakami, H. J. Snaith, *Science* **2012**, *338*, 643.
- [5] Y. Ogomi, A. Morita, S. Tsukamoto, T. Saitho, N. Fujikawa, Q. Shen, T. Toyoda, K. Yoshino, S. S. Pandey, T. Ma, S. Hayase, *J. Phys. Chem. Lett.* **2014**, *5*, 1004.

- [6] W. S. Yang, J. H. Noh, N. J. Jeon, Y. C. Kim, S. Ryu, J. Seo, S. I. Seok, *Science* **2015**, 348, 1234.
- [7] N. J. Jeon, J. H. Noh, W. S. Yang, Y. C. Kim, S. Ryu, J. Seo, S. I. Seok, *Nature* **2015**, 517, 476.
- [8] G. Han, S. Zhang, P. P. Boix, L. H. Wong, L. Sun, S.-Y. Lien, *Prog. Mater. Sci.* **2017**, 87, 246.
- [9] D. Bi, C. Yi, J. Luo, J. D. Décoppet, F. Zhang, S. M. Zakeeruddin, X. Li, A. Hagfeldt, M. Grätzel, *Nat. Energy* **2016**, 1, 16142.
- [10] T. Ye, S. Ma, X. Jiang, L. Wei, C. Vijila, S. Ramakrishna, *Adv. Funct. Mater.* **2017**, 27, 1606545.
- [11] National Renewable Energy Laboratory (NREL), Research Cell Efficiency Records, <https://www.nrel.gov/pv/assets/images/efficiency-chart.png> (accessed: December 2017).
- [12] G. Grancini, C. Roldán-Carmona, I. Zimmermann, E. Mosconi, X. Lee, D. Martineau, S. Narbey, F. Oswald, F. D. Angelis, M. Graetzel, M. K. Nazeeruddin, *Nat. Commun.* **2017**, 8, 15684.
- [13] C. C. Stoumpos, C. D. Malliakas, M. G. Kanatzidis, *Inorg. Chem.* **2013**, 52, 9019.
- [14] X. Lü, Y. Wang, C. C. Stoumpos, Q. Hu, X. Guo, H. Chen, L. Yang, J. S. Smith, W. Yang, Y. Zhao, H. Xu, *Adv. Mater.* **2016**, 28, 8663.
- [15] H. S. Jung, N. G. Park, *Small* **2015**, 11, 10.
- [16] A. M. A. Leguy, Y. Hu, M. Campoy-Quiles, M. I. Alonso, O. J. Weber, P. Azarhoosh, M. v. Schilfgaarde, M. T. Weller, T. Bein, J. Nelson, P. Docampo, P. R. F. Barnes, *Chem. Mater.* **2015**, 27, 3397.
- [17] R. J. Sutton, G. E. Eperon, L. Miranda, E. S. Parrott, B. A. Kamino, J. B. Patel, M. T. Hörlantner, M. B. Johnston, A. A. Haghighirad, D. T. Moore, H. J. Snaith, *Adv. Energy Mater.* **2016**, 5, 1502458.
- [18] B. Conings, J. Drijkoningen, N. Gauquelin, A. Babayigit, J. D'Haen, L. D'Olieslaeger, A. Ethirajan, J. Verbeeck, J. Manca, E. Mosconi, F. D. Angelis, H.-G. Boyen, *Adv. Energy Mater.* **2016**, 5, 1500477.
- [19] T. M. Koh, B. Febriansyah, N. Mathews, *Chem* **2017**, 2, 326.
- [20] I. C. Smith, E. T. Hoke, D. Solis-Ibarra, M. D. McGehee, H. I. Karunadasa, *Angew. Chem.* **2014**, 126, 11414.
- [21] T. M. Koh, V. Shanmugam, J. Schlipf, L. Oesinghaus, P. Müller-Buschbaum, N. Ramakrishnan, V. Swamy, N. Mathews, P. P. Boix, S. G. Mhaisalkar, *Adv. Mater.* **2016**, 28, 3653.
- [22] H. Tsai, W. Nie, J. C. Blancon, C. C. Stoumpos, R. Asadpour, B. Harutyunyan, A. J. Neukirch, R. Verduzco, J. J. Crochet, S. Tretiak, L. Pedesseau, *Nature* **2016**, 536, 312.
- [23] Z. Wang, Q. Lin, F. P. Chmiel, N. Sakai, L. M. Herz, H. J. Snaith, *Nat. Energy* **2017**, 2, 17135.
- [24] B. Yang, S. Xiao, C. Hu, T. Zhang, X. Meng, H. Lin, Y. Yang, S. Yang, *Adv. Energy Mater.* **2017**, 7, 1701038.
- [25] F. Wang, W. Geng, Y. Zhou, H. H. Fang, C. J. Tong, M. A. Loi, L. M. Liu, N. Zhao, *Adv. Mater.* **2016**, 28, 9986.
- [26] C. Y. Ma, C. Q. Leng, Y. X. Ji, X. Z. Wei, K. Sun, L. L. Tang, J. Yang, W. Luo, C. L. Li, Y. S. Deng, S. L. Feng, J. Shen, S. R. Lu, C. L. Du, H. F. Shi, *Nanoscale* **2016**, 8, 18309.
- [27] D. H. Cao, C. C. Stoumpos, O. K. Farha, J. T. Hupp, M. G. Kanatzidis, *J. Am. Chem. Soc.* **2015**, 137, 7843.
- [28] H. H. Tsai, W. Y. Nie, J. C. Blancon, C. C. S. Stoumpos, R. Asadpour, B. Harutyunyan, A. J. Neukirch, R. Verduzco, J. J. Crochet, S. Tretiak, L. Pedesseau, J. Even, M. A. Alam, G. Gupta, J. Lou, P. M. Ajayan, M. J. Bedzyk, M. G. Kanatzidis, A. D. Mohite, *Nature* **2016**, 536, 312.
- [29] Y. Lin, Y. Bai, Y. Fang, Z. Chen, S. Yang, X. Zheng, S. Tang, Y. Liu, J. Zhao, J. Huang, *J. Phys. Chem. Lett.* **2018**, 9, 654.
- [30] T. Ye, X. Wang, X. Li, A. Q. Yan, S. Ramakrishna, J. Xu, *J. Mater. Chem. C* **2017**, 5, 1255.
- [31] B. Russ, A. Glaudell, J. J. Urban, M. L. Chabiny, A. S. Rachel, *Nat. Rev. Mater.* **2016**, 1, 16050.
- [32] A. Pisoni, J. Jacimovic, O. S. Barišić, M. Spina, R. Gaál, F. László, E. Horváth, *J. Phys. Chem. Lett.* **2014**, 5, 2488.
- [33] T. Ye, X. Jiang, D. Wan, X. Wang, J. Xing, T. Venkatesan, Q. Xiong, S. Ramakrishna, *ChemPhysChem* **2016**, 17, 4102.
- [34] Y. Yamada, T. Nakamura, M. Endo, A. Wakamiya, Y. Kanemitsu, *J. Am. Chem. Soc.* **2014**, 136, 11610.
- [35] S. D. Stranks, V. M. Burlakov, T. Leijtens, J. M. Ball, A. Goriely, H. J. Snaith, *Phys. Rev. Appl.* **2014**, 2, 034007.
- [36] T. Ye, J. Xing, M. Petrovi, S. Chen, V. Chellappan, G. S. Subramanian, T. C. Sum, B. Liu, Q. Xiong, S. Ramakrishna, *Sol. Energy Mater. Sol. Cells* **2017**, 163, 242.
- [37] B. Li, M. Li, C. Fei, G. Cao, J. Tian, *J. Mater. Chem. A* **2017**, 5, 24168.
- [38] C. Fei, B. Li, R. Zhang, H. Fu, J. Tian, G. Cao, *Adv. Energy Mater.* **2017**, 7, 1602017.
- [39] A. Mei, X. Li, L. Liu, Z. Ku, T. Liu, Y. Rong, M. Xu, M. Hu, J. Chen, Y. Yang, M. Grätzel, H. Han, *Science* **2014**, 345, 295.